Rapid Communication

Surface analysis of mixed-conducting ferrite membranes by the conversion-electron Mössbauer spectroscopy

J.C. Waerenborgh [a], E.V. Tsipis [a], A.A. Yaremchenko [b], V.V. Kharton [b],*

[a] Chemistry Department, Instituto Tecnológico e Nuclear, CFMC-UL, EN 10, 2686-953 Sacavém, Portugal
[b] Department of Ceramics and Glass Engineering, CICECO, University of Aveiro, 3810-193 Aveiro, Portugal

ARTICLE INFO

ABSTRACT

Conversion-electron Mössbauer spectroscopy analysis of iron surface states in the dense ceramic membranes made of ^{57}Fe-enriched $SrFe_{0.7}Al_{0.3}O_{3-\delta}$ perovskite, shows no traces of reductive decomposition or carbide formation in the interfacial layers after operation under air/CH_4 gradient at 1173 K, within the limits of experimental uncertainty. The predominant trivalent state of iron cations at the membrane permeate-side surface exposed to flowing dry methane provides evidence of the kinetic stabilization mechanism, which is only possible due to slow oxygen-exchange kinetics and enables long-term operation of the ferrite-based ceramic reactors for natural gas conversion. At the membrane feed-side surface exposed to air, the fractions of Fe^{4+} and Fe^{3+} are close to those in the powder equilibrated at atmospheric oxygen pressure, suggesting that the exchange limitations to oxygen transport are essentially localized at the partially reduced surface.

1. Introduction

Dense ceramic membranes with mixed oxygen-ionic and electronic conductivity make it possible to combine oxygen separation from air and partial oxidation of methane (POM) in a single reactor, providing substantial benefits compared to the conventional technologies for natural gas conversion [1–3]. A high level of oxygen permeability and relatively good thermomechanical properties are known for ferrite-based perovskite phases which exhibit, however, insufficient thermodynamic stability in the CH_4 conversion products, H_2 and CO. In theory, bulk reduction of the ferrite-based membranes under air/CH_4 gradient may be prevented due to oxygen surface-exchange limitations at the membrane permeate side, leading to a higher oxygen chemical potential in the surface layers with respect to gaseous phase [1,3], as illustrated by inset in Fig. 1. This kinetic stabilization mechanism is in agreement with numerous results of the membrane bulk characterization after operation, including X-ray diffraction (XRD) and scanning electron microscopy (SEM) [1,3]. Experimental information on the iron surface states in the ferrite-based mixed conductors and on their role in CH_4 oxidation processes is still very scarce. Contrary to other transition metal-containing oxide materials that are catalytically active for the

total combustion of hydrocarbons, examples of a high catalytic activity of perovskite-related ferrites toward POM at temperatures above 970 K were documented in the literature (e.g. [3–8]). Possible hypotheses ascribed this phenomenon to the strongly-bonded lattice oxygen with low mobility, to a presence of carbonate species on the surface, and to formation of catalytically active species such as iron carbide or metallic Fe [4–7]. The coulometric titration and transmission Mössbauer spectroscopy (TMS) in combination with pulse catalytic studies showed that increasing POM selectivity is observed in the vicinity of the state where iron cations in the perovskite-like lattice are predominantly trivalent and extensive oxygen-vacancy ordering starts to occur [8].

The present work was focused on the evaluation of iron states in the surface layers of ferrite-based ceramic membranes after operation under air/CH_4 gradient by conversion-electron Mössbauer spectroscopy (CEMS). To the best of authors' knowledge, the CEMS technique is used in this area of solid state chemistry and electrochemistry for the first time. Although CEMS is a highly-selective and non-destructive method advantageous for these goals, its applications to bulky complex materials are rare as it requires the presence of large concentrations of ^{57}Fe in the subsurface layers [9,10]. The maximum depth analyzed by integral CEMS registering all electrons back-scattered from the surface is approximately 200–300 nm [9,10]. For recording the spectra, the concentration of ^{57}Fe at the surface and in the subsurface layers should be at least $\sim 10^{14}$ atoms/cm^2, while its

---

natural abundance is only 2.2 at% [9,10]. Therefore, CEMS data are usually collected for iron-rich compositions, for ^{57}Fe-doped thin films, or when ^{57}Fe is implanted into surfaces. In this work, CEMS was applied to study surface states in the dense ceramic membranes of ^{57}Fe-enriched $SrFe_{0.7}Al_{0.3}O_{3-\delta}$ perovskite, selected as a prototype membrane composition due to substantially high oxygen permeability and attractive catalytic properties [3,8]. Comparison is made with the TMS data collected using the powdered samples annealed in various atmospheres, which were partly reported earlier [11] and re-analyzed in the present work.

2. Experimental

Single-phase $SrFe_{0.7}Al_{0.3}O_{3-\delta}$ powders, containing natural iron and enriched with ^{57}Fe, were synthesized by the glycine-nitrate process (GNP) as described elsewhere [3]. For the preparation of ^{57}Fe-rich materials, the stoichiometric amount of metallic iron with 95.7% ^{57}Fe isotope (chemical purity 99.96%, Chemgas, France) was dissolved in diluted nitric acid and then added into solution containing other metal cations, used for the GNP. After annealing of the synthesized powders at 1073 K, gas-tight ceramic membranes (density $>93\%$) were pressed and sintered in air at 1520–1570 K. The powdered samples used for XRD and TMS analyses were obtained by grinding of sintered ceramics and subsequent equilibration in various conditions, specified below. The powders equilibrated in air were either slowly cooled (1–2 K/min) down to room temperature or quenched in liquid nitrogen. Another series of the powdered samples were treated in flowing H_2–H_2O–N_2 mixture at 1023 K or CH_4 at 1173 K for 22 h, followed by fast cooling (10 K/min) in the same flow. The oxygen partial pressure ($p(O_2)$) in the H_2–H_2O–N_2 mixture monitored by an electrochemical oxygen sensor was approximately 10^{-17} atm; this oxygen activity was selected on the basis of phase stability limits [3] in order to provide equilibration in moderately reducing conditions and to avoid phase decomposition. For the membrane studies in flowing CH_4, dense $Sr^{57}Fe_{0.7}Al_{0.3}O_{3-\delta}$ ceramic discs were polished and hermetically attached onto a quartz tube used in the model reactor by a glass–ceramic sealant based on strontium–barium aluminosilicate. The reactor configuration, relevant equipment and procedures were described elsewhere [3]. Dry CH_4 ($\geq 99.995\%$ purity, 2 ml/min flow rate) was supplied onto the permeate-side surface (effective geometric area of 65 ± 1 mm^2), whilst the feed-side surface of the membrane was exposed to atmospheric air, such that oxygen permeated through the $Sr^{57}Fe_{0.7}Al_{0.3}O_{3-\delta}$ disc and reacted with methane. Testing under air/CH_4 gradient was performed at 1173 K during 22 h; then the reactor was quenched under the same gradient and the membrane was removed for examination by CEMS, XRD, SEM and energy-dispersive spectroscopy (EDS). The testing time of 22 h was selected on the basis of preliminary experiments, which showed complete decomposition of $SrFe_{0.7}Al_{0.3}O_{3-\delta}$ powder under similar conditions (Fig. 1 bottom). On the other hand, this period of time is short enough to avoid significant effects of other factors, such as kinetic demixing of the membrane and carbon deposition in the reactor due to thermal CH_4 cracking (see [1–3] and references cited), that may cause phase separation, gas diffusion limitations and reactor fracture.

Description of the equipment used for materials characterization and properties of perovskite-type $SrFe_{0.7}Al_{0.3}O_{3-\delta}$, including performance of the dense ceramic membranes for CH_4 conversion, are found in the previous publications [3,8,11]. The transmission Mössbauer (TM) spectra were collected at room temperature and at 4–15 K using a conventional constant-acceleration spectrometer equipped with a 25 mCi ^{57}Co source in a Rh matrix (Wissel). The CEMS analysis of the ceramic membranes was performed at room

temperature, with the sample mounted inside a proportional back-scatter detector RIKON-5 (Wissel) in a flowing 5% CH_4–95% He gas mixture. The CEM and TM spectra were fitted to Lorentzian lines using a non-linear least-squares method. Distributions of magnetic splittings were fitted according to the histogram method; the relative areas and widths of peaks 1–6, 2–5 and 3–4 in each magnetic sextet were kept equal during refinement. In this work, all isomer shifts (IS) are given relative to α-Fe at 295 K.

3. Results and discussion

XRD and TMS analyses confirmed that $SrFe_{0.7}Al_{0.3}O_{3-\delta}$ perovskite remains stable in a relatively wide range of the oxygen chemical potentials varying from oxidizing down to mildly reducing in a H_2–H_2O–N_2 flow (Figs. 1–3). The relevant Mössbauer behaviour was analyzed elsewhere [11]; in this brief communication, one should only note that under oxidizing conditions, Fe^{3+} and Fe^{4+} are present, whereas reducing oxygen chemical potential leads to progressive lowering of the iron oxidation states and coordination numbers (Table 1). Nonetheless, the conversion-electron Mössbauer (CEM) spectrum of the $Sr^{57}Fe_{0.7}Al_{0.3}O_{3-\delta}$ membrane surface exposed to air (feed side) is the mirror image of the 295 K transmission spectrum of the bulk $SrFe_{0.7}Al_{0.3}O_{3-\delta}$ sample equilibrated in air, within the limits of experimental error (Fig. 2A and B). Very similar fractions of Fe^{3+} and Fe^{4+} were derived from the CEM and TM spectra, Table 1. This behaviour
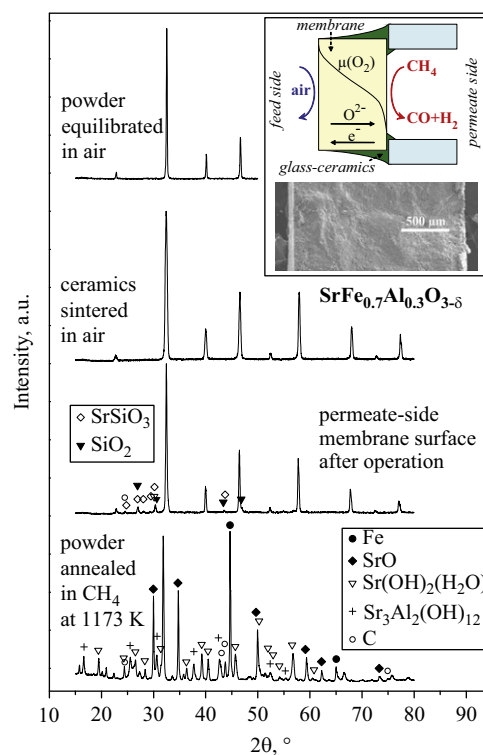
Fig. 1. XRD patterns (from top to bottom): $SrFe_{0.7}Al_{0.3}O_{3-\delta}$ powder equilibrated in atmospheric air, surface of as-sintered ceramics, permeate-side surface of the ceramic membrane after operation under air/CH_4 gradient at 1173 K tested by CEMS, and powder annealed in flowing CH_4 at 1173 K for 22 h. For $SrSiO_3$ and carbon, the marked peaks correspond to the PDF files 241232/360018 and 10742330/501085, respectively. Inset shows a part of experimental setup for the membrane testing under air/CH_4 gradient where a dense membrane disk is hermetically attached to a quartz tube by glass–ceramic sealant (top), and SEM micrograph of one $SrFe_{0.7}Al_{0.3}O_{3-\delta}$ membrane fractured after operation, illustrating an absence of bulk decomposition (bottom). Solid line in the inset shows theoretical distribution of the oxygen chemical potential, $\mu(O_2)$, across a mixed-conducting membrane with surface-limited oxygen transport.
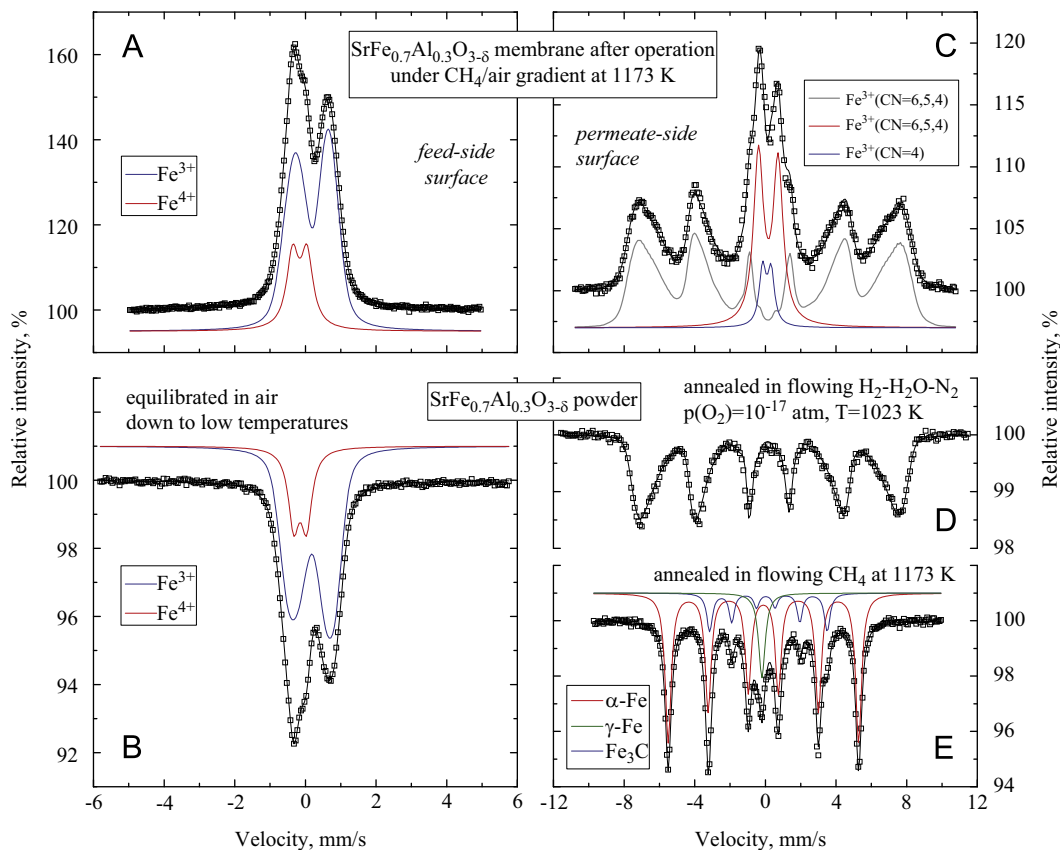
Fig. 2. Room-temperature CEM spectra of Sr^{57}Fe$_{0.7}$Al$_{0.3}$O$_{3-\delta}$ membrane feed- (A) and permeate- (C) side surfaces after testing under CH$_4$/air gradient at 1173 K for 22 h, and TM spectra of SrFe$_{0.7}$Al$_{0.3}$O$_{3-\delta}$ powders: equilibrated at low temperatures with atmospheric oxygen (B), annealed in a H$_2$–H$_2$O–N$_2$ flow at p(O$_2$)$=10^{-17}$ atm and 1023 K (D), and annealed in flowing CH$_4$ at 1173 K during 22 h (E). The lines plotted over the experimental points are the sum of quadrupole doublets and hyperfine field distributions shown shifted for clarity.

indicates that the oxygen chemical potential at the feed-side surface of the ceramic membranes operating under air/CH$_4$ gradient is close to the atmospheric one. Therefore, the surface exchange limitations to oxygen transport, indicated by the membrane thickness dependencies of steady-state oxygen permeation fluxes [11], are essentially localized at the permeate side. The latter factor is critically important for the kinetically stable operation of the ferrite-based membranes [1,3].

An opposite situation is observed in CH$_4$-containing atmospheres. When powdered Sr^{57}Fe$_{0.7}$Al$_{0.3}$O$_{3-\delta}$ interacts with methane and products of its oxidation by the lattice oxygen, the perovskite phase partly decomposes and segregation of metallic Fe occurs (Fig. 1), in agreement with thermodynamic stability boundaries [3]. The corresponding TM spectra collected at room temperature and at 4 K (Figs. 2E and 3B) both consist of two magnetic sextets and one central absorption peak. The sextet parameters (Table 1) are characteristic of α-Fe and iron carbide [12]. At 295 K the central absorption peak can be fitted by a single line with IS of −0.08 mm/s; at 4 K this peak becomes much broader and a sextet with weak magnetic hyperfine field (B_{hf}) provides much better accuracy. The low B_{hf} ($\sim$2 T) at 4 K, and low IS values at 295 and 4 K are all typical for γ-Fe. Although pure γ-Fe is only stable above $\sim$1185 K, the incorporation of even few C atoms significantly lowers this temperature [13]. Indeed, traces of coking were detected by XRD (Fig. 1). On the contrary, CEM spectrum of the permeate-side surface of Sr^{57}Fe$_{0.7}$Al$_{0.3}$O$_{3-\delta}$ membrane exposed to CH$_4$ displays a pair of emission peaks superimposed on a sextet of extremely broad lines (Fig. 2C). This sextet is comparable to the absorption sextets observed in the room-temperature TM spectrum of mildly reduced SrFe$_{0.7}$Al$_{0.3}$O$_{3-\delta}$

powder (Fig. 2D). Broadening may originate from relaxation effects associated with the proximity of the temperature where long-range magnetic correlations are established and with the presence of non-magnetic Al^{3+} in the Fe^{3+} sites [14]. In order to simulate the magnetic relaxation [15,16] a B_{hf} distribution was fitted to the CEMS and TMS data. The same average B_{hf} values were estimated for the membrane permeate-side surface and for the partially reduced material annealed in H$_2$–H$_2$O–N$_2$ (Table 1). In these distributions the IS values decrease from 0.36 mm/s down to 0.23 mm/s with decreasing B_{hf} from 50 to 15 T, which is indicative of coexistence of 6-, 5- and 4-folds coordinated Fe^{3+}. The latter conclusion is validated by the analysis of TM spectra collected at 4 K (Fig. 3A) when the magnetic relaxation is negligible. The central emission peaks in the membrane CEM spectrum (Fig. 2C) have different intensities and a reasonable agreement may only be achieved considering two quadrupole doublets, which were attributed again to Fe^{3+} in several coordinations but with lower average coordination, and to tetra-coordinated Fe^{3+}. The presence of these doublets absent in the 295 K TM spectra reflects faster relaxation for a fraction of Fe^{3+} at the membrane/gas interface. This difference originates from lower effective dimensionality of the system [14,17], leading to lower magnetic ordering temperature in a thin layer compared to the bulk. For instance, the Neél temperature in FeBO$_3$ crystals was found to gradually decrease across a 300 nm surface layer [17].

Whatever the microscopic factors responsible for Fe^{3+} behaviour, no traces of metallic Fe, carbide species and even Fe^{2+} cations were detected at the Sr^{57}Fe$_{0.7}$Al$_{0.3}$O$_{3-\delta}$ membrane surface exposed to CH$_4$ flow, within the limits of experimental uncertainty. In particular, a peak at −5.3 mm/s and a shoulder at

-3.1 mm/s would be observed in the CEM spectrum (Fig. 2C) in case of α-Fe segregation. If assuming the same peak widths as those in Fig. 2E, the signal with 3–5% intensity should be already
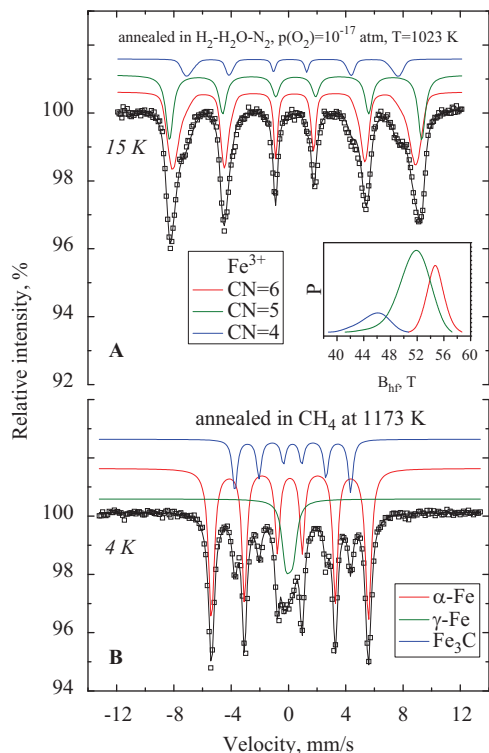
Fig. 3. Low-temperature TM spectra of SrFe$_{0.7}$Al$_{0.3}$O$_{3-\delta}$ equilibrated in a H$_2$–H$_2$O–N$_2$ flow at $p(O_2)=10^{-17}$ atm and 1023 K (A), and annealed in flowing CH$_4$ at 1173 K (B). The lines plotted over the experimental points are the sum of three hyperfine field distributions (A) or three magnetic sextets (B) shown shifted for clarity. Inset shows the probability distribution of the magnetic hyperfine fields.

detectable. For Fe^{2+} in wustite-based phases [18], an additional peak at approximately 1.4 mm/s can be expected to appear in the CEM spectrum. As these characteristic peaks are absent, the fractions of possible reduction products, such as metallic iron and/or Fe$_{1-\gamma}$O, in the near-surface layer of Sr^{57}Fe$_{0.7}$Al$_{0.3}$O$_{3-\delta}$ membrane are smaller than 3–4% if any. The secondary peaks visible in the XRD pattern of the permeate-side membrane surface examined by CEMS (Fig. 1) can all be ascribed to SiO$_2$ and silicate phases in the glass–ceramic sealant at the membrane edges (see inset in Fig. 1). Although the sealant traces cannot be safely removed without destroying the membrane as its mechanical strength becomes low after quenching under air/CH$_4$ gradient, no peaks characteristic of Fe metal or binary iron oxides are
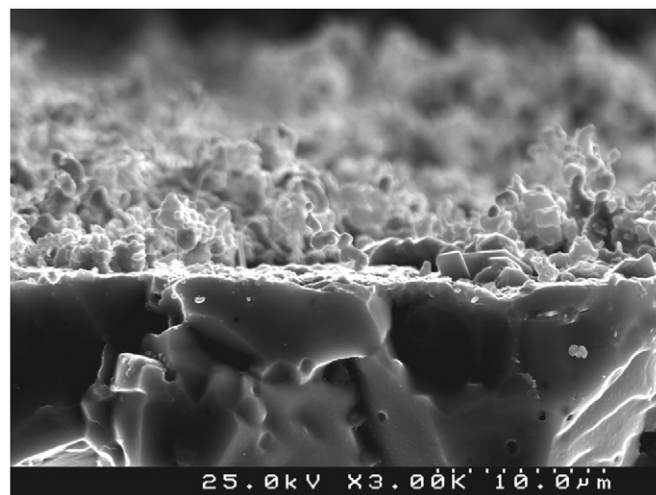
Fig. 4. SEM micrograph of a fractured SrFe$_{0.7}$Al$_{0.3}$O$_{3-\delta}$ membrane with porous Pt catalyst deposited onto permeate-side surface (top), after exposure to flowing dry CH$_4$ during 55 h.

Table 1
Parameters[a] estimated from the CEM spectra of Sr^{57}Fe$_{0.7}$Al$_{0.3}$O$_{3-\delta}$ ceramic membrane after testing under air/dry CH$_4$ gradient and TM spectra of SrFe$_{0.7}$Al$_{0.3}$O$_{3-\delta}$ powders after annealing in various atmospheres.

Sample/conditions	Technique	T (K)	IS (mm/s)	QS, 2ε (mm/s)	B_{hf} (T)	I (%)	Fe species	Reference
Membrane after operation at 1173 K, feed (air) side	CEMS	295	0.29	0.96	–	77	Fe^{3+}	This work
			-0.04	0.41	–	23	Fe^{4+}	
Powder equilibrated in air, $p(O_2)=0.21$ atm, $T=295$ K	TMS	295	0.29	1.02	–	79	Fe^{3+}	[11]
			-0.04	0.36	–	21	Fe^{4+}	
		15	0.43	-0.02	44.2	75	Fe^{3+}	[11]
			0.12	-0.16	22.3	25	Fe^{4+}	
Membrane after operation at 1173 K, permeate (CH$_4$) side	CEMS	295	0.32[b]	-0.01	40.3[b]	67	Fe^{3+}(CN=6,5,4)	This work
			0.20	0.48	–	6	Fe^{3+}(CN=4)	
			0.28	1.11	–	27	Fe^{3+}(CN=6,5,4)	
Powder equilibrated at $p(O_2)=10^{-17}$ atm and $T=1023$ K	TMS	295	0.32[b]	0.00	40.5[b]	100	Fe^{3+}	This work
		4	0.52	0.00	54.6	33	Fe^{3+}(CN=6)	This work
			0.43	-0.04	51.7	51	Fe^{3+}(CN=5)	
			0.22	0.16	45.3	16	Fe^{3+}(CN=4)	
Powder annealed in CH$_4$, $T=1173$ K	TMS	295	0.00	0.00	33.4	75	α-Fe	This work
			-0.08	–	–	10	γ-Fe	
			0.21	0.14	20.6	15	Fe$_3$C	
		4	0.12	0.00	34.0	67	α-Fe	This work
			0.07	0.00	2.1	14	γ-Fe	
			0.31	0.01	25.1	19	Fe$_3$C	

[a] IS, QS, 2ε, B_{hf} and I are the isomer shift relative to metallic α-Fe at 295 K, average quadrupole splitting estimated for the distributions of quadrupole doublets, quadrupole shift for magnetic sextets, magnetic hyperfine field and relative area, respectively. The estimated errors are ≤ 0.02 mm/s for IS, QS and ε, < 0.2 T for B_{hf} and $< 2\%$ for I. CN is the oxygen coordination number of iron cations.
[b] Average values; IS decreases with decreasing B_{hf} from 0.36 mm/s ($B_{hf}=50$ T) down to 0.23 mm/s ($B_{hf}=15$ T).

found in the XRD patterns. The conclusion drawn from the CEMS results was also qualitatively supported by SEM/EDS inspections; one example illustrating an absence of significant decomposition of $SrFe_{0.7}Al_{0.3}O_{3-\delta}$ ceramics with porous Pt catalyst deposited onto the permeate-side surface to promote POM reaction, is presented in Fig. 4.

In summary, the CEMS analysis of ferrite-based membrane surface layers shows that no reductive decomposition occurs in the dry methane oxidation regime, within the detection limits. This provides direct experimental evidence for the kinetic stabilization mechanism [1,3], enabling operation of the ferrite-based membrane reactors under the POM conditions when the perovskite phase is thermodynamically unstable. The predominant trivalent state of iron cations in the surface layer exposed to flowing dry CH_4, in combination with the absence of metallic and carbide species, throws light also on the catalytic reaction mechanisms of methane oxidation over dense ferrite-based membranes. Namely, the reaction kinetics seems primarily governed by oxygen desorption from the ferrite surface and, therefore, $Fe^{3+}-O^{2-}$ bonding strength rather than perovskite decomposition products segregated at the surface.

Acknowledgments

References

[1] P.V. Hendriksen, P.H. Larsen, M. Mogensen, F.W. Poulsen, K. Wiik, Catal. Today 56 (2000) 283.
[2] J. Sunarso, S. Baumann, J.M. Serra, W.A. Meulenberg, S. Liu, Y.S. Lin, J.C. Diniz da Costa, J. Membr. Sci. 320 (2008) 13.
[3] V.V. Kharton, A.A. Yaremchenko, A.A. Valente, V.A. Sobyanin, V.D. Belyaev, G.L. Semin, S.A. Veniaminov, E.V. Tsipis, A.L. Shaula, J.R. Frade, J. Rocha, Solid State Ionics 176 (2005) 781.
[4] A.G. Andersen, T. Hayakawa, M. Shimizu, K. Suzuki, K. Tokehira, Catal. Lett. 23 (1994) 59.
[5] R. Li, C. Yu, S. Shen, J. Natural Gas Chem. 11 (2002) 137.
[6] V.A. Sadykov, L.A. Isupova, I.S. Yakovleva, G.M. Alikina, A.I. Lukashevich, S. Neophytides, React. Kinet. Catal. Lett. 81 (2004) 393.
[7] F. Martinez-Ortega, C. Batiot-Dupeyrat, G. Valderrama, J.-M. Tatibouët, C.R. Acad. Sci. IIC 4 (2001) 49.
[8] V.V. Kharton, M.V. Patrakeev, J.C. Waerenborgh, V.A. Sobyanin, S.A. Veniaminov, A.A. Yaremchenko, P. Gaczyński, V.D. Belyaev, G.L. Semin, J.R. Frade, Solid State Sci. 7 (2005) 1344.
[9] J.R. Gancedo, J.Z. Dávalos, M. Gracia, J.F. Marco, Hyperfine Interact. 110 (1997) 41.
[10] K. Nomura, Y. Ujihira, A. Vértes, J. Radioanal. Nucl. Chem. 202 (1996) 103.
[11] V.V. Kharton, J.C. Waerenborgh, D.P. Rojas, A.A. Yaremchenko, A.A. Valente, A.L. Shaula, M.V. Patrakeev, F.M.B. Marques, J. Rocha, Catal. Lett. 99 (2005) 249.
[12] P. Coquay, E. DeGrave, R.E. Vandenberghe, A. Peigney, Ch. Laurent, Hyperfine Interact. 139/140 (2002) 289.
[13] R. Reed-Hill, R. Abbaschian, Physical Metallurgy Principles, third ed., PWS-Kent Publishing, Boston, 1991.
[14] T.C. Gibb, A.J. Herod, S.T. Lees, P.D. Battle, J. Mater. Chem. 5 (1995) 285.
[15] D. Predoi, V. Kuncser, E. Tronc, M. Nogues, U. Russo, G. Principi, G. Filoti, J. Phys.: Condens. Matter 15 (2003) 1797.
[16] Z. Klencsár, Z. Németh, E. Kuzmann, Z. Homonnay, A. Vértes, J. Hakl, K. Vad, S. Mészáros, A. Simopoulos, E. Devlin, G. Kallias, J.M. Grenéche, Á. Cziráki, S.K. De, J. Magn. Magn. Mater. 320 (2008) 651.
[17] A.S. Kamzin, B. Stahl, E. Kankeleit, R. Gellert, M. Muller, D.B. Vcherashnĭ, JETP Lett. 71 (2000) 442.
[18] D.P. Dobson, N.S. Cohen, Q.A. Pankhurst, J.P. Brodholt, Am. Mineral. 83 (1998) 794.